HHS Public Access

Author manuscript

Angew Chem Int Ed Engl. Author manuscript; available in PMC 2017 November 21.

Published in final edited form as:

Angew Chem Int Ed Engl. 2016 November 21; 55(48): 15058–15061. doi:10.1002/anie.201608539.

HNO Binding in Heme Proteins: Effects of Iron Oxidation State, Axial Ligand, and Protein Environment

Dr. Rahul L. Khade,

Department of Biomedical Engineering, Chemistry and Biological Sciences, Stevens Institute of Technology, 1 Castle Point on Hudson Hoboken, NJ 07030 (USA)

Yuwei Yang,

Department of Biomedical Engineering, Chemistry and Biological Sciences, Stevens Institute of Technology, 1 Castle Point on Hudson Hoboken, NJ 07030 (USA)

Yelu Shi, and

Department of Biomedical Engineering, Chemistry and Biological Sciences, Stevens Institute of Technology, 1 Castle Point on Hudson Hoboken, NJ 07030 (USA)

Prof. Dr. Yong Zhang

Department of Biomedical Engineering, Chemistry and Biological Sciences, Stevens Institute of Technology, 1 Castle Point on Hudson Hoboken, NJ 07030 (USA)

Yong Zhang: yong.zhang@stevens.edu

Abstract

HNO plays significant roles in many biological processes. Numerous heme proteins bind HNO, an important step for its biological functions. A systematic computational study was performed to provide the first detailed trends and origins of the effects of iron oxidation state, axial ligand, and protein environment on HNO binding. Results show that HNO binds much weaker with ferric porphyrins than corresponding ferrous systems, offering strong thermodynamic driving force for experimentally observed reductive nitrosylation. Axial ligand was found to influence HNO binding through its trans effect and charge donation effect. The protein environment significantly affects the HNO hydrogen bonding structures and properties. The predicted NMR and vibrational data are in excellent agreement with experiment. These novel and broad range of results shall facilitate studies of HNO binding in many heme proteins, models, and related metalloproteins.

Graphical Abstract

Correspondence to: Yong Zhang, yong.zhang@stevens.edu.

Supporting information for this article is given via a link at the end of the document.

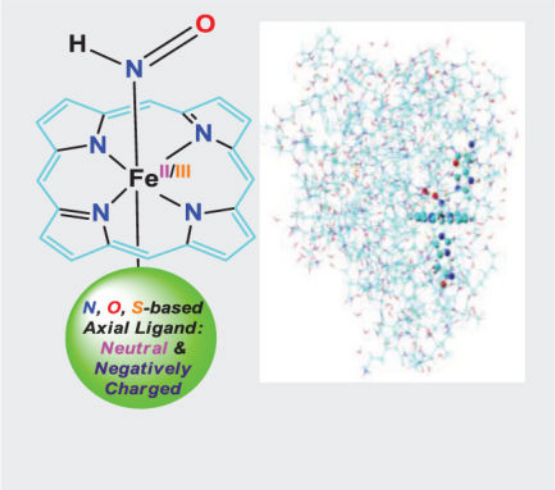

HNO binding is an important step for its biological functions. Our results for the first time directly show that 1) HNO preferably binds with ferrous porphyrins than corresponding ferric systems due to better metal to ligand back-donation; 2) Axial ligand can strongly influence HNO binding through its *trans* effect and charge donation effect; 3) The heme protein environment has a significant effect on HNO hydrogen bonding structures and properties in different proteins.

Keywords

nitrogen oxides; bioinorganic chemistry; heme proteins; porphyrinoids; density functional calculations

HNO plays significant roles in many biological processes, such as vascular relaxation, enzyme activity regulation, and neurological function regulation.[1] With a better vasodilative effect than NO and an increased contractility effect, HNO donors offer a promising new class of vasodilators and heart failure treatment.[2] It was also suggested as a potential treatment for reduction of neuron damage during stroke.[1a] Among its biological targets, heme proteins have been studied for several decades, such as nitrite and nitric oxide reductases involved in denitrification processes in plants, bacteria, and fungi,[1b, c] nitric oxide synthase, peroxidase, and cytochrome P450 nitric oxide reductase involving HNO as an intermediate in their catalytic cycles,[3] and metmyoglobin, methemoglobin, ferricytochrome *c*, oxymyoglobin, myoglobin, cytochrome P450, and horseradish peroxidase (HRP) used to scavenge HNO.[1a] Despite decades-long experimental work and recent computational work on geometric and electronic structures, affinities, spectroscopic properties of HNO bound protein complexes and models,[4] some critical questions remain to be answered. For instance, although it is well-known that ferrous nitrosyl compounds are more stable than corresponding ferric systems,[1a] such comparison of iron oxidation state on HNO binding has not been reported. Stable HNO binding was reported for several ferrous heme proteins,[5] but ferric hemes lead to reductive nitrosylation.[1a, 3c, 6] Despite this transient HNO binding in ferric hemes, the detailed comparisons of iron oxidation state on HNO binding may offer useful thermodynamic trend to help understand experimental results

and what properties are most significantly affected. In addition, given the different axial ligands in numerous heme proteins, how such axial ligand affects HNO binding is yet to be uncovered. The effect from the protein environment beyond the proximal axial ligand and distal hydrogen bonding residue is also unknown. Therefore, a systematic computational study was performed here to address these questions.

As the first study to address such questions, our goal is to reveal HNO binding trends due to these effects and their origins, not accurate absolute values of binding energies. So, the HNO bound ferrous and ferric porphyrins with five axial ligands (see Scheme 1) were first studied using the previously reported DFT method for similar systems[4b, c] in full geometry optimization and frequency analysis (trends are the same when other methods and solvent effect were used, see Supporting Information for computational details and optimized 3D structures). The 5-methylimidazole (5-MeIm), NH_2CH_3, PhO^-, and CH_3S^- ligands were used to model the axial His, Lys, Tyr, and Cys ligands in myoglobin, cytochrome c nitrite reductase, catalase, cytochrome P450 nitric oxide reductase, respectively, while CH_3O^- was used to compare with PhO^- and CH_3S^-. Since there is a strong correlation between HNO binding electronic energies (ΔE's) and Gibbs free energies (ΔG's) with linear correlation coefficient R^2=0.9885 (see Table S2 and Figure S1), the following discussion is based on ΔG's.

We first investigated the iron oxidation state effect. As shown in Table 1 and Figure 1, for all axial ligands studied here, HNO always preferably binds with ferrous porphyrins than corresponding ferric ones. It is interesting to note that the HNO binding ΔG's between ferric and ferrous porphyrins are highly correlated with R^2=0.9863, see Figure S2, suggesting a consistent iron oxidation state effect. This effect is the same as in the case of NO binding, [1a] which may not be surprising since the major driving force for HNO and NO binding in metalloporphyrins was recently found to be the same: metal back-donation to the anti-bonding π^*_{NO} orbital.[4c, d] However, this is the first time to directly show the iron oxidation state effect on HNO binding and the mostly influenced properties as described below. The weakened binding in ferric hemes are clearly demonstrated by their longer Fe-N(H)O distances (R_{FeN}'s) in Table 1, compared to ferrous systems. Based on this major driving force, the higher oxidation state leads to decreased metal back-donation to HNO, and consequently less negative NO charges (Q_{NO}'s), shorter NO bond lengths (R_{NO}'s), and larger NO vibrational frequencies (ν_{NO}'s), see Table 1. The strong interrelationships among R_{NO}, Q_{NO}, and ν_{NO} are shown in Figure 2A and 2B with R^2=0.9819 and 0.9881, respectively. Since this major electronic driving force involves mostly Fe to NO back-donation, we can see large geometric changes in R_{FeN} of ~0.04 Å and R_{NO} of ~0.03 Å (Table 1) vs. small changes in NH bond lengths (≤ 0.003 Å) and Fe-NO bond angles (≤ 2.3°) (Table S2) due to the iron oxidation state change.

The relatively weak HNO binding in ferric porphyrins offers the first theoretical insight to support a facile thermodynamic driving force for reductive nitrosylation to generate the stable NO bound ferrous porphyrins when HNO meets with ferric heme proteins and models, as observed experimentally with rate constants on the orders of 10^4~10^7 M^{-1} s^{-1}.[1a, 3c, 6] The varied reaction rates show that different proteins modulate the HNO

interactions. Since HNO binding is the first and rate-limiting step in such interactions,[1a] it is important to study more details of protein effect in this process.

We next investigated the protein axial ligand effect on HNO binding, since this proximal residue can vary in different heme proteins, and is directly attached to Fe and *trans* to HNO, which may play a significant role in regulating HNO binding. Indeed, as shown in Figure 1, there is a clear difference between neutral and negatively charged ligands regarding their effects on HNO binding, as highlighted by green and orange ovals respectively. The average HNO binding ΔG's for negatively charged ligands in both ferrous and ferric porphyrins are ca. 7–8 kcal/mol higher than those for neutral ligands, indicating less stable binding. This is probably a result of the stronger *trans* effect of negatively charged ligands compared to neutral ligands, as evidenced by their relatively longer Fe-N(H)O distances with an average of ~0.04 Å, see Table 1. It is interesting to note that experimental HNO consumption rates of ferric heme proteins with neutral His axial ligands (e.g. Mb, HRP) are higher than that of catalase with a negatively charged Tyr ligand.[3c] Since HNO binding is the first and rate-limiting step in such reactions,[1a] these experimental results suggest a favourable HNO binding with the neutral protein axial ligand, consistent with the trend revealed here.

Interestingly, axial ligand also has another effect: charge donation to metal center, resulting in positive ligand charge change upon HNO binding (ΔQ_L), see Table 1. These data show that a negatively charged ligand usually donates more charge than a neutral ligand. This enhances metal to HNO back-donation, resulting in a lengthened NO bond, increased NO charge, and smaller NO vibrational frequency as seen from Table 1. This effect is secondary compared to the above-mentioned *trans* effect of axial ligands with different formal charges on HNO binding. But it helps understand the mild difference for ligands with the same formal charge: a mildly improved HNO binding for NH_2CH_3 vs. 5-MeIm among neutral ligands, and for the sulfur ligand vs. the oxygen ligand among negatively charged ligands, due to their slightly stronger charge donation, see ΔQ_L data in Table 1.

Besides the proximal axial ligand, the distal hydrogen bonding residue was previously found to play an important role on HNO binding.[4b] However, the effects from other active site residues and the whole protein environment on HNO binding have not been reported. Because stable HNO binding was only reported for several ferrous heme proteins with spectroscopic characterizations,[5] we next used monomeric ferrous globins, myoglobin (Mb) and leghemoglobin (lgHb), with experimental ^1H and ^{15}N NMR spectroscopic data that are sensitive to differentiate various HNO binding modes,[4b] as the first step to examine these effects.

For Mb, we first studied large active site models with nearby residues that might influence HNO binding (see Supporting Information for details and optimized coordinates). Because both H and O of HNO can participate in hydrogen bonding (HB) and distal His can be either Nδ or Nε protonated, two mono HB modes (**A** – HNO···His, **B** – ONH···His) and two dual HB modes (**C** – H_2O···HNO···His, **D** – OH_2···ONH···His) were investigated. The use of water as the second HB partner in dual HB modes was based on our recent small active site model study: [4b] 1) only dual HB modes can reproduce experimental spectroscopic data, 2) the dual HB mode for HNO is actually common in previously reported HNO interactions,[4a]

and 3) water is viable in proteins and no other nearby residue in Mb can be the second HB partner. Since Mb and lgHb have same axial ligand and distal His residue, it is important to study the large active site to learn the origin of their experimental NMR shift differences.[5b] As seen from Table 2, mode **D** (see Figure 3A) consistently yields the best predictions of experimental ^{1}H and ^{15}N NMR chemical shifts for the major MbHNO isomer shown here,[5b] and its slightly larger NMR shifts than those of **C** is also consistent with the experimental results that this major isomer has slightly larger shifts than a minor isomer discussed previously.[4b] The predicted ν_{NO} value also agrees well with experiment.[5c] For lgHb, again mode **D** gives the best predictions of experimental NMR data and the slightly downfield ^{1}H and ^{15}N NMR shifts in lgHbHNO vs. MbHNO.[5b]

Above results show that the large active site models are helpful to study experimental spectroscopic data in Mb and lgHb. We then used such structures to reveal most significant differences in their HNO binding geometries. As shown in Table S3, the Fe-N(H)O distance, NO and NH bond lengths, and the Fe-N-O bond angle differences in each mode of these two proteins are all negligible (<0.005 Å and <1°). In contrast, HB geometries have much larger differences and the largest changes occur with HNO's HB with water. As seen from Table 2, from MbHNO to lgHbHNO, the average HNO···water distance (R_{water}) decreases as significant as ~0.07 Å, in contrast with ~0.01 Å difference in the average absolute HNO···His distances (R_{His}'s). This is probably due to the relatively smaller flexibility of distal His vs. water. These data also indicate a more compact active site in lgHbHNO. In fact, this feature is also reflected by the closest distances of nearby residues to HNO's O atom involved in water HB: 3.03/5.21 Å for Leu65/Val105 in lgHbHNO vs. 4.43/5.69 Å for Leu29/Val68 in MbHNO. In addition, as shown in Figure 3A and 3B, the water's H atom not involved in HB is pushed away from Leu65 in lgHbHNO compared to the toward Leu29 conformation in MbHNO, due to ~1.4 Å closer Leu in lgHbHNO. These results show that the nearby residues in the large active site models induce the structural differences between these two heme proteins, with changes mostly on HB geometries.

To compare with large active site models, the whole protein models for MbHNO were also investigated (see Supporting Information for computational details with one structure shown in Figure 3C). As shown in Table S3, again the optimized R_{FeN}, R_{NO}, R_{NH}, and <FeNO data are basically not affected with only <0.01 Å and <1° differences. The significant geometric changes are also associated with HNO's HB distances, with the water side HB again more affected than the distal His side.

In summary, this work provides the first detailed trends and origins of effects of iron oxidation state, axial ligand, and protein environment on HNO binding in heme proteins: 1) ferric hemes have much weaker binding than ferrous systems due to reduced metal back-donation to HNO, offering the first theoretical insight into the strong thermodynamic driving force for experimentally observed reductive nitrosylation to form stable NO bound ferrous porphyrins; 2) axial ligand influences HNO binding through its *trans* effect and charge donation effect, providing the first information how its formal charge and structural feature affects HNO binding; 3) the protein environment effect of other active site residues and whole protein was also revealed for the first time, with significant changes on HNO's HB structures and properties, and is responsible for experimental spectral differences in different

heme proteins. These novel and broad range of results shall facilitate many researches of HNO binding in heme proteins, models, and related metalloproteins.

Supplementary Material

Refer to Web version on PubMed Central for supplementary material.

Acknowledgments

This work was supported by an NIH grant GM085774 to YZ. YZ also thanks Liu Yang for her preliminary study of this project.

References

1. a) Miranda KM. Coord Chem Rev. 2005; 249:433–455.b) Averill BA. Chem Rev. 1996; 96:2951–2964. [PubMed: 11848847] c) Farmer PJ, Sulc F. J Inorg Biochem. 2005; 99:166–184. [PubMed: 15598500] d) Roncaroli F, Videla M, Slep LD, Olabe JA. Coord Chem Rev. 2007; 251:1903–1930.e) Flores-Santana W, Switzer C, Ridnour LA, Basudhar D, Mancardi D, Donzelli S, Thomas DD, Miranda KM, Fukuto JM, Wink DA. Arch Pharm Res. 2009; 32:1139–1153. [PubMed: 19727606] f) Doctorovich F, Bikiel D, Pellerino J, Suarez SA, Larsen A, Marti MA. Coord Chem Rev. 2011; 255:2764–2784.g) Doctorovich F, Bikiel DE, Pellegrino J, Suárez SA, Martí MA. Acc Chem Res. 2014; 47:2907–2916. [PubMed: 25238532]
2. Feelisch M. Proc Natl Acad Sci - U S A. 2003; 100:4978–4980. [PubMed: 12704227]
3. a) Rusche KM, Spiering MM, Marletta MA. Biochemistry. 1998; 37:15503–15512. [PubMed: 9799513] b) Huang JM, Sommers EM, Kim-Shapiro DB, King SB. J Am Chem Soc. 2002; 124:3473–3480. [PubMed: 11916434] c) Miranda KM, Paolocci N, Katori T, Thomas DD, Ford E, Bartberger MD, Espey MG, Kass DA, Feelisch M, Fukuto JM, Wink DA. Proc Natl Acad Sci U S A. 2003; 100:9196–9201. [PubMed: 12865500] d) Lehnert N, Praneeth VKK, Paulat F. J Comput Chem. 2006; 27:1338–1351. [PubMed: 16788909]
4. a) Zhang Y. J Inorg Biochem. 2013; 118:191–200. [PubMed: 23103077] b) Yang L, Ling Y, Zhang Y. J Am Chem Soc. 2011; 133:13814–13817. [PubMed: 21834502] c) Ling Y, Mills C, Weber R, Yang L, Zhang Y. J Am Chem Soc. 2010; 132:1583–1591. [PubMed: 20078039] d) Yang L, Fang WH, Zhang Y. Chem Comm. 2012; 48:3842–3844. [PubMed: 22437041] e) Linder DP, Rodgers KR. Inorg Chem. 2005; 44:8259–8264. [PubMed: 16270963] f) Goodrich LE, Lehnert N. J Inorg Biochem. 2013; 118:179–186. [PubMed: 23146743] g) Goodrich LE, Roy S, Alp EE, Zhao J, Hu MY, Lehnert N. Inorg Chem. 2013; 52:7766–7780. [PubMed: 23746143] h) Speelman AL, Lehnert N. Acc Chem Res. 2014; 47:1106–1116. [PubMed: 24555413] i) Einsle O, Messerschmidt A, Huber R, Kroneck PMH, Neese F. J Am Chem Soc. 2002; 124:11737–11745. [PubMed: 12296741] j) Silaghi-Dumitrescu R. Eur J Inorg Chem. 2003:1048–1052.
5. a) Kumar MR, Fukuto JM, Miranda KM, Farmer PJ. Inorg Chem. 2010; 49:6283–6292. [PubMed: 20666387] b) Kumar MR, Pervitsky D, Chen L, Poulos T, Kundu S, Hargrove MS, Rivera EJ, Diaz A, Colon JL, Farmer PJ. Biochemistry. 2009; 48:5018–5025. [PubMed: 19368336] c) Immoos CE, Sulc F, Farmer PJ, Czarnecki K, Bocian DF, Levina A, Aitken JB, Armstrong RS, Lay PA. J Am Chem Soc. 2005; 127:814–815. [PubMed: 15656601] d) Sulc F, Fleischer E, Farmer PJ, Ma DJ, La Mar GN. J Biol Inorg Chem. 2003; 8:348–352. [PubMed: 12589571] e) Lin R, Farmer PJ. J Am Chem Soc. 2000; 122:2393–2394.
6. a) Bari SE, Marti MA, Amorebieta VT, Estrin DA, Doctorovich F. J Am Chem Soc. 2003; 125:15272–15273. [PubMed: 14664554] b) Marti MA, Bari SE, Estrin DA, Doctorovich F. J Am Chem Soc. 2005; 127:4680–4684. [PubMed: 15796534] c) Álvarez L, Suarez SA, Bikiel DE, Reboucas JS, Batini-Haberle I, Martí MA, Doctorovich F. Inorg Chem. 2014; 53:7351–7360. [PubMed: 25001488]

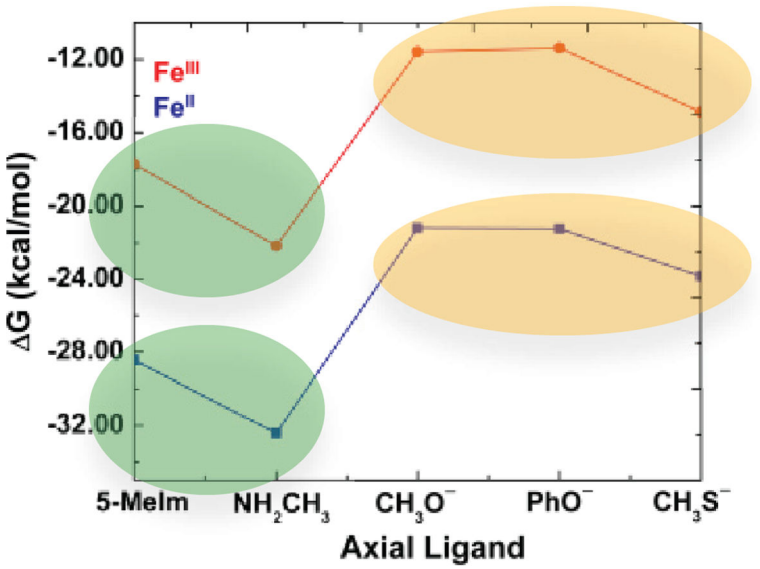

Figure 1.

Binding Gibbs free energies of HNO complexes **1–10**. Red and blue data points are for ferric and ferrous complexes, respectively.

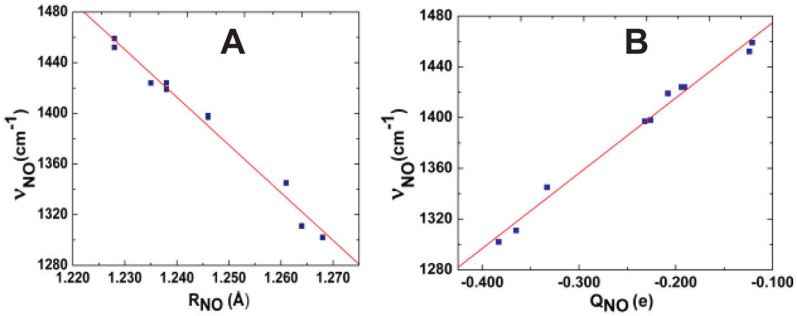

Figure 2.
Plots of ν_{NO} vs. R_{NO} (**A**) and ν_{NO} vs. Q_{NO} (**B**) for complexes **1–10**.

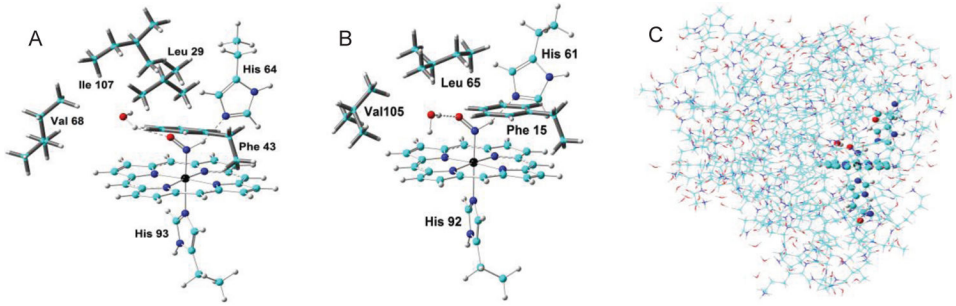

Figure 3.

HB mode **D** structures of (**A**) large active site of MbHNO; (**B**) large active site of lgHbHNO; (**C**) MbHNO whole protein. Atom color scheme: C- cyan, N- blue, O- red, H – grey, Fe - black.

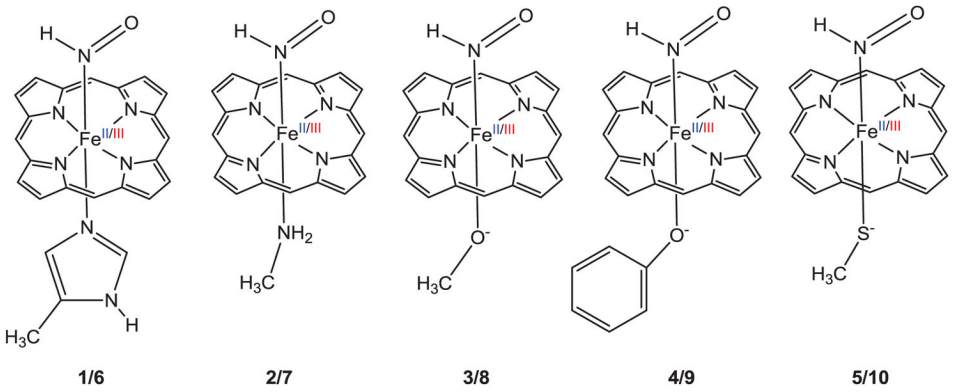

Scheme 1.

Molecular structures of studied HNO complexes of ferrous (**1–5**) and ferric (**6–10**) porphyrins.

Table 1

Binding Energies, Geometric Parameters, Charges, and Vibrational Frequencies of $Fe^{II/III}$(Por)(HNO)(L) [a]

	L	ΔG (kcal/mol)	R_{FeN} (Å)	R_{NO} (Å)	Q_{NO} (e)	ΔQ_L (e)	υ_{NO} (cm^{-1})
Fe^{II}	5-MeIm	−28.44	1.805	1.246	−0.226	0.093	1398
	NH_2CH_3	−32.40	1.804	1.246	−0.232	0.095	1397
	CH_3O^-	−21.20	1.852	1.268	−0.383	0.108	1302
	PhO^-	−21.24	1.823	1.261	−0.333	0.075	1345
	CH_3S^-	−23.84	1.862	1.264	−0.365	0.138	1311
Fe^{III}	5-MeIm	−17.71	1.848	1.228	−0.124	0.094	1452
	NH_2CH_3	−22.17	1.845	1.228	−0.121	0.103	1459
	CH_3O^-	−11.57	1.893	1.238	−0.208	0.189	1419
	PhO^-	−11.36	1.842	1.238	−0.191	0.241	1424
	CH_3S^-	−14.86	1.904	1.235	−0.194	0.293	1424

[a] L = axial ligand.

Table 2

Geometric Parameters and Spectroscopic Properties of HNO bound heme proteins

	[a]	HB Mode	R_{His} (Å)	R_{water} (Å)	δ_H (ppm)	δ_N (ppm)	υ_{NO} (cm^{-1})
Mb	Expt *[b]*				14.93	661	1385
	Small *[c]*	**A**	2.176	/	14.93	605	1377
		B	2.078	/	15.55	659	1402
		C	2.145	2.031	15.04	647	1380
		D	2.069	2.095	15.13	658	1384
	Large	**A**	2.118	/	14.86	604	1374
		B	2.068	/	15.84	661	1396
		C	2.095	2.118	15.02	644	1377
		D	2.014	2.104	15.05	663	1374
	Whole	**A**	2.160	/	14.66	600	1380
		B	2.055	/	15.45	657	1397
		C	2.107	2.033	15.04	642	1383
		D	1.999	1.960	15.30	662	1374
LgHb	Expt *[d]*				15.00	665	
	Large	**A**	2.126	/	14.85	605	1374
		B	2.049	/	15.65	662	1392
		C	2.085	2.044	14.84	649	1379
		D	2.031	2.037	15.48	666	1376

*[a]*Small, Large, and Whole represent small active site models, large active site models, and whole protein, respectively.

*[b]*Refs. 5a–c.

*[c]*Ref.4b.

*[d]*Ref. 5b.